

ENHANCED MICROPLANE CONCRETE MODEL

T. Hasegawa,
Institute of Technology, Shimizu Corporation,
Tokyo, Japan

Abstract

The previously developed Microplane Concrete Model is improved to expand its applicability and reconstructed into the Enhanced Microplane Concrete Model as a more general constitutive law. One of the main improvements is to take account of resolved lateral stress (resolved lateral component of the macroscopic stress tensor) in normal compression response on the microplane. Another main improvement is to adapt a transition model from brittle to ductile fracture for shear response on the microplane with increasing resolved normal compression stress (resolved normal compression component of the macroscopic stress tensor). Those improvements bring the model a complicated interaction effect between microplanes through macroscopic stress tensor. It is verified that the Enhanced Microplane Concrete Model can predict well experimental constitutive relations of concrete from references.

1 Introduction

The microplane model has been shown to be effective for describing constitutive relations and damage of concrete material. The primitive model has a clear physical image in the microscopic level, and it is based on a

characteristic hypothesis that the inelastic origin of concrete as a heterogeneous material is microcracks which occur within the interface region (microplane) between the mortar matrix and large aggregate. However, some of the previous models lose the conceptual clearness of the microplane to expand their applicability. Bazant and Gambarova (1984) developed the normal component formulation model in which an additional elastic body was incorporated with the microplane system for adjusting Poisson's ratio. The recent models by Bazant and Prat (1988), Ozbolt and Bazant (1992), and Carol et al. (1991) adapted volumetric-deviatoric-shear component formulation to obtain an arbitrary Poisson's ratio. It seem to go against the basic hypothesis of the microplane model to split microplane responses into an overall macroscopic response and each microplane response.

In view of the previous microplane models losing conceptual clearness, Hasegawa and Bazant (1993) reconstructed the Microplane Concrete Model (MPC Model) so that no additional elastic body or volumetric component of microplane was used for adjusting Poisson's ratio. In the present study the previously developed MPC Model is improved to expand its applicability and reconstructed into the Enhanced Microplane Concrete Model (EMPC Model) as a more general constitutive law for concrete.

2 Formulation

2.1 Hypotheses

By contrast with the microplane model by Bazant and Prat (1988), the normal strain component on the microplane in the EMPC Model is not split into volumetric and deviatoric parts. The following are the hypotheses in the present model.

Hypothesis I : Normal strain ϵ_N , shear strains ϵ_{TK} , ϵ_{TM} , and lateral strain ϵ_L of a microplane are the resolved components of the macroscopic strain tensor ϵ_{ij} (tensorial kinematic constraint).

Hypothesis II : Normal stress σ_N and shear stresses σ_{TK} , σ_{TM} on a microplane depend on normal strain ϵ_N and shear strains ϵ_{TK} , ϵ_{TM} . The relations between those strains and stresses are described by microconstitutive laws.

Hypothesis III : The normal stress increment on a microplane depends on the resolved lateral strain ϵ_L (lateral strain effect) and resolved lateral stress S_L (lateral stress effect) on the same microplane as well (additional static constraint).

Hypothesis IV : The inelastic shear stress increment on a microplane depends on the resolved normal component S_N of the macroscopic stress tensor σ_{ij} on the same microplane (additional static constraint).

Hypothesis V : The microconstitutive laws for the normal and shear components are based on a generalized Maxwell rheologic model in

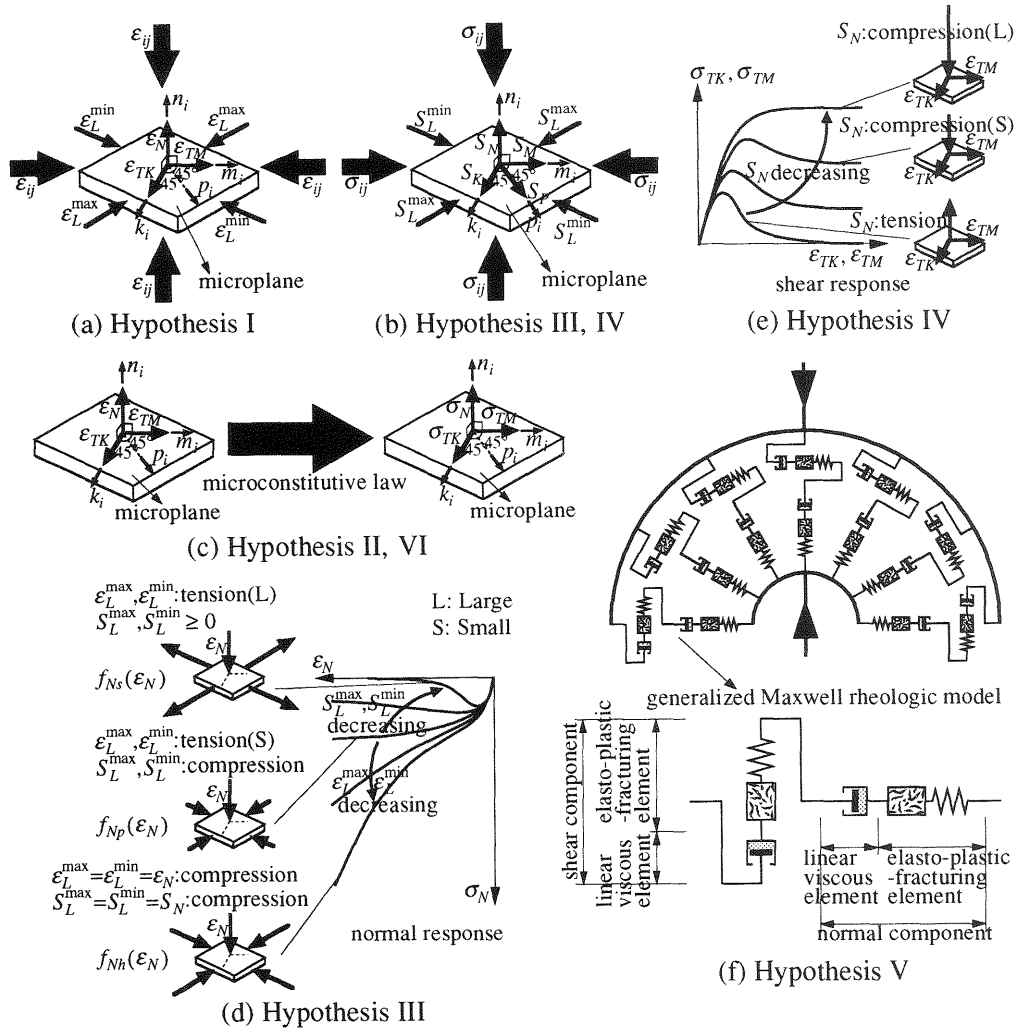


Fig.1. Hypotheses of Enhanced Microplane Concrete Model

which a linear viscous element is coupled in series with an elasto-plastic-fracturing element.

Hypothesis VI : The microconstitutive laws for the normal and shear components on each microplane are mutually independent.

Fig.1 represents the hypotheses.

According to hypothesis I, normal strain ϵ_N and shear strains $\epsilon_{TK}, \epsilon_{TM}$ on a microplane of direction cosines n_i are

$$\epsilon_N = n_j n_k \epsilon_{jk} \quad (1)$$

$$\epsilon_{TK} = \frac{1}{2} (k_i n_j + k_j n_i) \epsilon_{ij}; \quad \epsilon_{TM} = \frac{1}{2} (m_i n_j + m_j n_i) \epsilon_{ij} \quad (2)$$

where k_i and m_i are components of in-plane unit coordinate vectors \mathbf{k} , \mathbf{m} normal to each other as shown in Fig.1. They are determined as described in Hasegawa and Bazant (1993).

The maximum and minimum principal values $\epsilon_L^{\max}, \epsilon_L^{\min}$ of lateral strain

on each microplane are evaluated to implement hypothesis III.

$$\varepsilon_L^{\max} = \frac{\varepsilon_K + \varepsilon_M}{2} + \sqrt{\left(\frac{\varepsilon_K - \varepsilon_M}{2}\right)^2 + \left(\frac{\varepsilon_K + \varepsilon_M}{2} - \varepsilon_P\right)^2} \quad (3a)$$

$$\varepsilon_L^{\min} = \frac{\varepsilon_K + \varepsilon_M}{2} - \sqrt{\left(\frac{\varepsilon_K - \varepsilon_M}{2}\right)^2 + \left(\frac{\varepsilon_K + \varepsilon_M}{2} - \varepsilon_P\right)^2} \quad (3b)$$

in which $\varepsilon_K = k_i k_j \varepsilon_{ij}$, $\varepsilon_M = m_i m_j \varepsilon_{ij}$, and $\varepsilon_P = p_i p_j \varepsilon_{ij}$ are the lateral normal strains in the directions of \mathbf{k} , \mathbf{m} , and \mathbf{p} . The in-plane unit vector \mathbf{p} has 45° angles with \mathbf{k} and \mathbf{m} as shown in Fig.1.

The resolved normal component S_N of the macroscopic stress tensor σ_{ij} on a microplane whose direction cosines are n_i is

$$S_N = n_j \sigma_j^n = n_j n_k \sigma_{jk} \quad (4)$$

The maximum and minimum principal values S_L^{\max} , S_L^{\min} of resolved lateral stress on each microplane are

$$S_L^{\max} = \frac{S_K + S_M}{2} + \sqrt{\left(\frac{S_K - S_M}{2}\right)^2 + \left(\frac{S_K + S_M}{2} - S_P\right)^2} \quad (5a)$$

$$S_L^{\min} = \frac{S_K + S_M}{2} - \sqrt{\left(\frac{S_K - S_M}{2}\right)^2 + \left(\frac{S_K + S_M}{2} - S_P\right)^2} \quad (5b)$$

in which $S_K = k_i k_j \sigma_{ij}$, $S_M = m_i m_j \sigma_{ij}$, and $S_P = p_i p_j \sigma_{ij}$ are the resolved lateral normal stresses in the directions of \mathbf{k} , \mathbf{m} , and \mathbf{p} .

2.2 Normal-shear component formulation

The incremental microconstitutive relations are written separately for the normal component and the shear components in the K and M directions

$$d\sigma_N = C_N d\varepsilon_N - d\sigma_N'' = f_{N1}(\varepsilon_N, \varepsilon_L, S_L) = f_{N2}(\varepsilon_{kl}, \sigma_{kl}, n_r) \quad (6a)$$

$$d\sigma_{TK} = C_{TK} d\varepsilon_{TK} - d\sigma_{TK}'' = f_{T1}(\varepsilon_{TK}, S_N) = f_{T2}(\varepsilon_{kl}, \sigma_{kl}, n_r) \quad (6b)$$

$$d\sigma_{TM} = C_{TM} d\varepsilon_{TM} - d\sigma_{TM}'' = f_{T1}(\varepsilon_{TM}, S_N) = f_{T2}(\varepsilon_{kl}, \sigma_{kl}, n_r) \quad (6c)$$

in which C_N , C_{TK} , and C_{TM} : incremental elastic stiffnesses for the microplane; $d\sigma_N''$, $d\sigma_{TK}''$, and $d\sigma_{TM}''$: inelastic microplane stress increments; $f_{N1}(\varepsilon_N, \varepsilon_L, S_L)$ and $f_{N2}(\varepsilon_{kl}, \sigma_{kl}, n_r)$ are $d\sigma_N$ expressed in terms of ε_N , ε_L , and S_L , and in terms of ε_{kl} , σ_{kl} and n_r ; $f_{T1}(\varepsilon_{Ts}, S_N)$ and $f_{T2}(\varepsilon_{kl}, \sigma_{kl}, n_r)$ are $d\sigma_{Ts}$ expressed in terms of ε_{Ts} and S_N , and in terms of ε_{kl} , σ_{kl} , and n_r ($Ts = TK, TM$).

Using the principle of virtual work, we can write

$$\int_V d\sigma_{ij} \delta\varepsilon_{ij} dV = 2 \int_S (d\sigma_N \delta\varepsilon_N + d\sigma_{TK} \delta\varepsilon_{TK} + d\sigma_{TM} \delta\varepsilon_{TM}) f(\mathbf{n}) dS \quad (7)$$

in which $\delta\varepsilon_{ij}$, $\delta\varepsilon_N$, $\delta\varepsilon_{TK}$, and $\delta\varepsilon_{TM}$: small variations of macroscopic strain tensor and the strains on the microplane; V : the volume of unit sphere; S : the surface of unit hemisphere; $f(\mathbf{n})$: a weight function for the normal direction \mathbf{n} . Expressing $\delta\varepsilon_N$, $\delta\varepsilon_{TK}$, and $\delta\varepsilon_{TM}$ from (1) and (2), and substituting them as well as (6) into (7), we can get the macroscopic

incremental stress-strain relation

$$d\sigma_{ij} = C_{ijrs} d\epsilon_{rs} - d\sigma_{ij}'' \quad (8)$$

where C_{ijrs} denotes the incremental elastic stiffness tensor

$$C_{ijrs} = \frac{3}{2\pi} \int_S \left[n_i n_j n_r n_s C_N + \frac{1}{4} (k_i n_j + k_j n_i) (k_r n_s + k_s n_r) C_{TK} \right. \\ \left. + \frac{1}{4} (m_i n_j + m_j n_i) (m_r n_s + m_s n_r) C_{TM} \right] f(\mathbf{n}) dS \quad (9)$$

and $d\sigma_{ij}''$ denotes the inelastic stress increment

$$d\sigma_{ij}'' = \frac{3}{2\pi} \int_S \left[n_i n_j d\sigma_N'' + \frac{1}{2} (k_i n_j + k_j n_i) d\sigma_{TK}'' \right. \\ \left. + \frac{1}{2} (m_i n_j + m_j n_i) d\sigma_{TM}'' \right] f(\mathbf{n}) dS \quad (10)$$

Since $d\sigma_N$, $d\sigma_{TK}$, and $d\sigma_{TM}$ are the functions of strain tensor ϵ_{kl} and stress tensor σ_{kl} , the incremental stress tensor $d\sigma_{ij}$ can be written as

$$d\sigma_{ij} = \frac{3}{2\pi} \int_S \left[n_i n_j f_{N2}(\epsilon_{kl}, \sigma_{kl}, n_r) + \frac{1}{2} (k_i n_j + k_j n_i) f_{T2}(\epsilon_{kl}, \sigma_{kl}, n_r) \right. \\ \left. + \frac{1}{2} (m_i n_j + m_j n_i) f_{T2}(\epsilon_{kl}, \sigma_{kl}, n_r) \right] f(\mathbf{n}) dS \quad (11)$$

As you see from the fact that the incremental stress tensor depends on not only strain tensor but also stress tensor, interaction effect between microplanes is modeled in the EMPC Model through the additional static constraint. The interaction effect makes the present model deviate from the basic concept that individual microplane responses are independent from each other, which principally comes from the kinematic constraint. The effect is necessary to take account of a situation within concrete where microcracks, damage, and plasticity in each direction effect each other.

2.3 Microconstitutive law for normal component

The purpose of taking account of the lateral strain and stress effects on normal response of the microplane according to hypothesis III is to achieve the following (Fig.1(d)):

1. The normal strain response would not be the same as the hydrostatic response except when the lateral strains ϵ_L are the same as the normal strain ϵ_N , which is the case of hydrostatic loading.
2. The normal response would have a plastic plateau when the difference between the normal strain ϵ_N and the lateral strain ϵ_L is large, and when the resolved lateral stress S_L of the microplane is a large, compressive value, i.e., it would exhibit ductile plasticity.
3. The normal response would be more brittle when the difference between the normal strain ϵ_N and the lateral strain ϵ_L is large, and when the resolved lateral stress S_L of the microplane is a small, compressive value or a tensile value, i.e., it would exhibit more strain softening.

For the lateral strain effect it is useful to introduce a lateral-deviatoric

strain ε_{LD} to define the difference between ε_N and ε_L

$$\varepsilon_{LD} = \left| \varepsilon_N - \varepsilon_L^{\max} \right| + \left| \varepsilon_N - \varepsilon_L^{\min} \right| \quad (12)$$

The following hardening-softening function $\phi(\varepsilon_{LD})$ in terms of ε_{LD} is introduced

$$\begin{aligned} \phi(\varepsilon_{LD}) &= \frac{1}{1 + (\varepsilon_{LD}/\varepsilon_{LD}^1)^m} && : \text{when } S_{LC} < 0 \\ &= \frac{1}{1 + (\varepsilon_{LD}^p/\varepsilon_{LD}^1)^m} = \phi^p && : \text{when } \varepsilon_{LD} = \varepsilon_{LD}^p \\ &= 0 && : \text{when } S_{LC} \geq 0 \end{aligned} \quad (13)$$

in which ε_{LD}^1 : ε_{LD} value when $\phi(\varepsilon_{LD}) = 0.5$; m : a constant that specifies the shape of the curve $\phi(\varepsilon_{LD})$; and ϕ^p : $\phi(\varepsilon_{LD})$ value corresponding to the case of plastic response.

To take account of the lateral stress effect on the normal response, the following lateral confinement stress S_{LC} is defined combining S_L^{\max} and S_L^{\min}

$$\begin{aligned} S_{LC} &= S_L^{\max} + S_L^{\min} && : \text{when } S_L^{\max} < 0 \text{ and } S_L^{\min} < 0 \\ &= 0 && : \text{when } S_L^{\max} \geq 0 \text{ and } S_L^{\min} < 0 \\ &= 0 && : \text{when } S_L^{\max} \geq 0 \text{ and } S_L^{\min} \geq 0 \\ &= 0 && : \text{when } S_N \geq 0 \text{ on any other microplane} \\ &= S_{LC}^p && : \text{when } S_{LC} \leq S_{LC}^p \end{aligned} \quad (14)$$

in which $S_{LC}^p \leq S_{LC} \leq 0$; S_{LC}^p : S_{LC} value corresponding to the case of plastic response.

Weight functions are set in terms of $\phi(\varepsilon_{LD})$ and S_{LC} and utilized to obtain a gradual transition from hydrostatic response to plastic response and softening response for the virgin loading curve of the normal component of the microplane (Fig.1(d))

when $1 \geq \phi(\varepsilon_{LD}) \geq \phi^p$ and any S_{LC}

$$\sigma_N(\varepsilon_N, \varepsilon_{LD}, S_{LC}) = \left(\frac{\phi(\varepsilon_{LD}) - \phi^p}{1 - \phi^p} \right) f_{Nh}(\varepsilon_N) + \left(\frac{1 - \phi(\varepsilon_{LD})}{1 - \phi^p} \right) f_{Np}(\varepsilon_N) \quad (15a)$$

when $\phi^p > \phi(\varepsilon_{LD}) \geq 0$ and $S_{LC} \leq S_{LC}^p$

$$\sigma_N(\varepsilon_N, \varepsilon_{LD}, S_{LC}) = f_{Np}(\varepsilon_N) \quad (15b)$$

when $\phi^p > \phi(\varepsilon_{LD}) \geq 0$ and $S_{LC}^p < S_{LC} < 0$

$$\sigma_N(\varepsilon_N, \varepsilon_{LD}, S_{LC}) = \left(\frac{S_{LC}}{S_{LC}^p} \right) f_{Np}(\varepsilon_N) + \left(\frac{S_{LC}^p - S_{LC}}{S_{LC}^p} \right) f_{Ns}(\varepsilon_N) \quad (15c)$$

when $\phi^p > \phi(\varepsilon_{LD}) \geq 0$ and $0 \leq S_{LC}$

$$\sigma_N(\varepsilon_N, \varepsilon_{LD}, S_{LC}) = f_{Ns}(\varepsilon_N) \quad (15d)$$

in which $f_{Nh}(\varepsilon_N)$: hydrostatic loading curve when $\phi(\varepsilon_{LD}) = 1$; $f_{Np}(\varepsilon_N)$: plastic loading curve when $\phi(\varepsilon_{LD}) = \phi^p$; and $f_{Ns}(\varepsilon_N)$: softening loading

curve when $\phi^p > \phi(\varepsilon_{LD}) \geq 0$ and $0 \leq S_{LC}$.

The loading tangential stiffness and linear unload-reload stiffness in normal compression of the microplane are formulated with the similar weight functions to the loading curves.

In the EMPC Model the same type of formulas as the MPC Model are used for tensile softening curve $f_{NT}(\varepsilon_N)$, compressive softening curve $f_{Ns}(\varepsilon_N)$, and hydrostatic curve $f_{Nh}(\varepsilon_N)$ of the normal component (Fig.1). On the other hand, unlike the MPC Model $f_{Np}(\varepsilon_N)$ is specified separately from $f_{Nh}(\varepsilon_N)$ in the present model.

2.4 Microconstitutive law for shear components

In the present model shear loading curves are defined individually for softening (subscript *TT*) under resolved normal tension stress, softening (subscript *TC*) under resolved normal compression stress, and plasticity (subscript *Tp*) under resolved normal compression stress. A shear friction law is applied to evaluate shear peak stress for pre- and postpeak curves under resolved normal tension stress and for prepeak curves under resolved normal compression stress. On the other hand, postpeak shear response under resolved normal compression stress is calculated weighting the softening and plasticity curves with resolved normal stress. This brings a transition model from brittle to ductile fracture for shear response on the microplane (Fig.1(e)).

when $S_N \leq S_N^p$

$$\sigma_T(\varepsilon_T, S_N) = f_{Tp}(\varepsilon_T) \quad (16a)$$

when $S_N^p < S_N < 0$ and in the prepeak

$$\sigma_T(\varepsilon_T, S_N) = f_{TC}(\varepsilon_T) = f_{Tp}(\varepsilon_T) \quad (16b)$$

when $S_N^p < S_N < 0$ and in the postpeak

$$\sigma_T(\varepsilon_T, S_N) = \left(\frac{S_N}{S_N^p} \right) f_{Tp}(\varepsilon_T) + \left(\frac{S_N^p - S_N}{S_N^p} \right) f_{TC}(\varepsilon_T) \quad (16c)$$

when $0 \leq S_N$

$$\sigma_T(\varepsilon_T, S_N) = f_{TT}(\varepsilon_T) \quad (16d)$$

in which $f_{Tp}(\varepsilon_T)$: plastic loading curve when $S_N \leq S_N^p$; $f_{TC}(\varepsilon_T)$ and $f_{TT}(\varepsilon_T)$: softening loading curves under resolved normal compression and tension stresses; S_N^p : S_N value when shear response becomes the plasticity curve.

The loading tangential stiffness and linear unload-reload stiffness in shear components of the microplane are formulated with the similar weight functions to the loading curves.

$f_{TC}(\varepsilon_T)$ and $f_{TT}(\varepsilon_T)$ are the same type of formulas as the shear softening curve used in the MPC Model. While the prepeak portion of $f_{Tp}(\varepsilon_T)$ is the same form as $f_{TC}(\varepsilon_T)$, a constant peak stress (perfect plasticity) is assumed after the peak.

The concept of shear frictional coefficient is utilized to model the

dependence of shear peak stress τ^0 on S_N .

For tension of shear ($\varepsilon_T > 0$)

$$\tau^0 = +\sigma_{TC}^0 - \mu_{TC}S_N \quad : \text{ when } S_N < 0 \quad (17a)$$

$$\tau^0 = +\sigma_{TT}^0 - \mu_{TT}S_N \geq +r_{\min}^0\sigma_{TT}^0 \quad : \text{ when } S_N \geq 0 \quad (17b)$$

For compression of shear ($\varepsilon_T < 0$)

$$\tau^0 = -\sigma_{TC}^0 + \mu_{TC}S_N \quad : \text{ when } S_N < 0 \quad (17c)$$

$$\tau^0 = -\sigma_{TT}^0 + \mu_{TT}S_N \leq -r_{\min}^0\sigma_{TT}^0 \quad : \text{ when } S_N \geq 0 \quad (17d)$$

in which $\sigma_{TT}^0 (> 0)$ and $\sigma_{TC}^0 (> 0)$: shear peak stresses at $S_N = 0$ under resolved normal tension and compression stresses; $\mu_{TT} (> 0)$ and $\mu_{TC} (> 0)$: shear frictional coefficients under resolved normal tension and compression stresses; r_{\min}^0 : a constant specifying a lower limit of shear peak stress under resolved normal tension stress ($0 < r_{\min}^0 \leq 1$).

2.5 Cyclic modeling for the microplane

The generalized Maxwell rheologic model for rate dependence and the exponential algorithm for stable numerical integration, which were introduced in Hasegawa and Bazant (1993), are utilized in the present model for each microplane.

The same cyclic modeling in microconstitutive law as the MPC Model are adopted: i.e., the loading-unloading-reloading criteria for microplane response; the microplane hysteresis rule using the concept of back-stress and objective-stress; the microplane alternating cyclic rule covering both the tensile and compressive stress range and general strain histories. However, back-stress is redefined separately for unloading and reloading to prevent hysteresis loop from becoming narrow. For hysteresis response of normal compression on the microplane, the lateral strain and stress effects are taken into account. Shear hysteresis response is formulated accounting for resolved normal compression stress on the microplane. The details are given in Hasegawa and Bazant (1993), and Hasegawa (1994).

3 Verification

3.1 Monotonic behavior

Stress-strain responses were calculated with the present EMPC Model to verify it. The integrations in (9) and (10) were evaluated using the numerical integration formula shown in Fig.2.

Fig.3 is the result of triaxial compression analyses along compressive meridian comparing with the experiments by Smith et al. (1989); σ_c and f_c' are the lateral confining pressure and the uniaxial compressive strength. The material parameter values are as follows: 1) For normal tension: $\sigma_{NT}^0 = 40 \text{ kgf/cm}^2$, $\zeta_{NT} = 0.5$, $\gamma_{NT} = 5.0$, $p_{NT} = 1.0$, and $\rho_{NT} = 10^5 \text{ sec}$; 2) for normal compression (softening): $\sigma_{NC}^0 = -400 \text{ kgf/cm}^2$, $\zeta_{NC} = 0.3$,

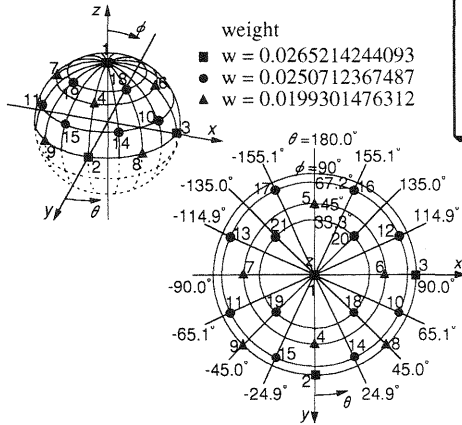


Fig.2. Numerical integration points on unit hemisphere

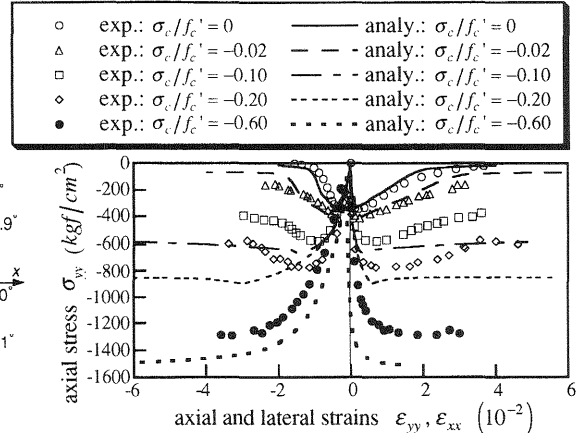
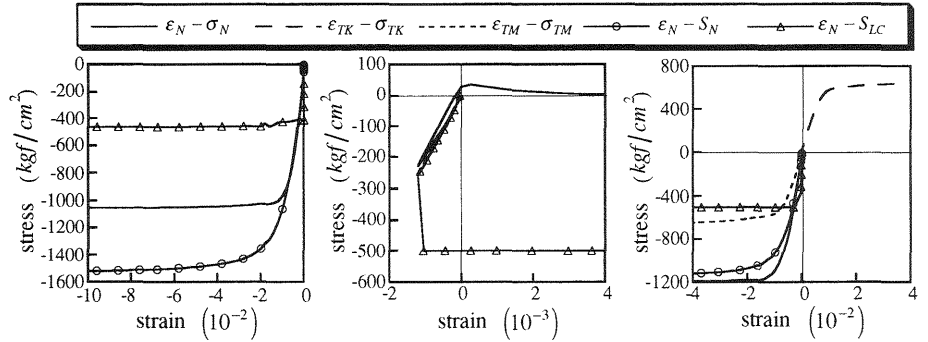


Fig.3. Triaxial compression analyses (compressive meridian)



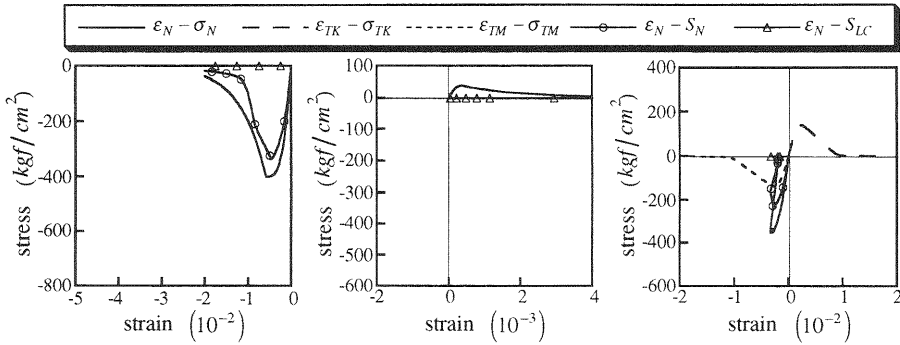
(a) microplane 2 (b) microplane 3 (c) microplane 14

Fig.4. Microplane responses for triaxial compression analysis ($\sigma_c / f_c' = -0.60$)

$\gamma_{NC} = 1.0$, $p_{NC} = 1.0$, and $\rho_{NC} = 10^7$ sec; 3) for normal compression (plasticity): $\sigma_{Np} = -1200 \text{ kgf/cm}^2$, and $\zeta_{Np} = 0.3$; 4) for shear under positive S_N : $\sigma_{TT}^0 = 17 \text{ kgf/cm}^2$, $\zeta_{TT} = 0.9$, $\gamma_{TT} = 0.5$, $p_{TT} = 1.0$, $\mu_{TT} = 4.0$, $r_{\min}^0 = 0.1$, and $\rho_{TT} = 10^6$ sec; 5) for shear under negative S_N : $\sigma_{TC}^0 = 17 \text{ kgf/cm}^2$, $\zeta_{TC} = 0.5$, $\gamma_{TC} = 1.0$, $p_{TC} = 1.0$, $\mu_{TC} = 0.6$, $S_N^p = -300 \text{ kgf/cm}^2$, and $\rho_{TC} = 10^6$ sec; 6) for lateral effects: $\epsilon_{LD}^1 = \epsilon_{LD}^p = 0.003$, $m = 1.0$, and $S_{LC}^p = -500 \text{ kgf/cm}^2$. The notations are given in Hasegawa (1994). These values are fixed for all the analyses in 3.1.

Figs.4 and 5 show the normal, K -shear, and M -shear responses of microplanes (integration points) 2, 3, and 14 for the triaxial ($\sigma_c / f_c' = -0.60$) and uniaxial ($\sigma_c / f_c' = 0$) compression analyses. From Figs.3-5 we can see that the present model is able to describe transition from brittle to ductile fracture and confinement effect, which is due to the rational modeling for responses on the microplane.

Triaxial compression behavior along tensile meridian was also well predicted with the EMPC Model as in Fig.6 where σ_h is the hydrostatic pressure.



(a) microplane 2 (b) microplane 3 (c) microplane 14
 Fig.5. Microplane responses for uniaxial compression analysis

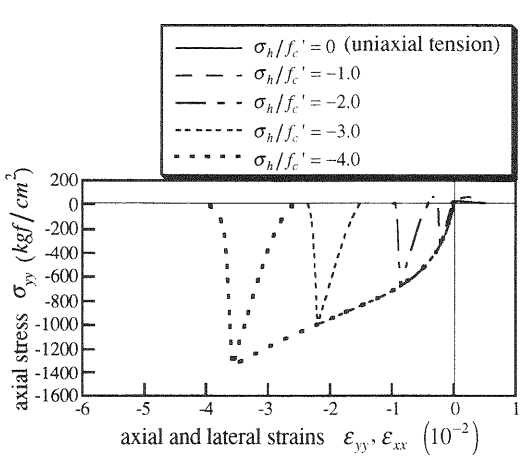


Fig.6. Triaxial compression analyses (tensile meridian)

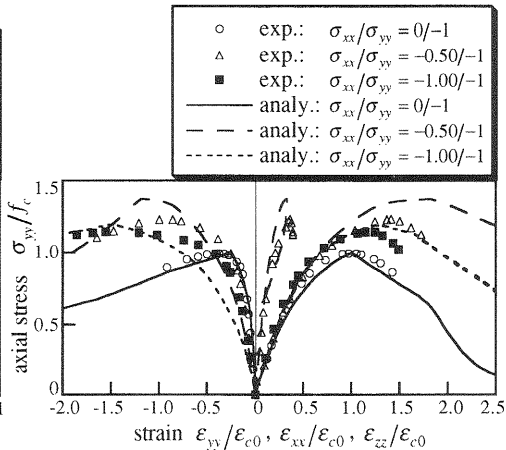


Fig.7. Biaxial compression analyses

In Figs.7 and 8 results of biaxial compression and compression-tension analyses are compared with experiments reported by Kupfer et al. (1969). ϵ_{c0} in those figures is the axial strain corresponding to f'_c . Relatively good agreement between the calculation and the experiment was achieved. The stress-strain responses under biaxial tension as well as uniaxial tension were also calculated and shown in Fig.9. The analytical responses under biaxial tension exhibit considerable nonlinearity in the prepeak regime, while the typical average stress-strain relations in experiments show almost perfect elasticity under biaxial tension. The present model is considered to evaluate nonlinear behavior in a highly localized damage region such as fracture process zone. Fig.10 shows the normal, K -shear, and M -shear responses of microplanes 2, 3, and 14 for the uniaxial tension analysis. Since the concept of shear frictional coefficient is applied under not only negative S_N but also positive S_N as in (17), shear responses on microplanes become small due to the large, tensile values of S_N in the uniaxial tension analysis (Fig.10). On the other hand, normal tensile damage on microplanes are prominent compared with shear damage, which suggests that tensile microcracks dominate the macroscopic fracture rather than shear (Mode II) microcracks

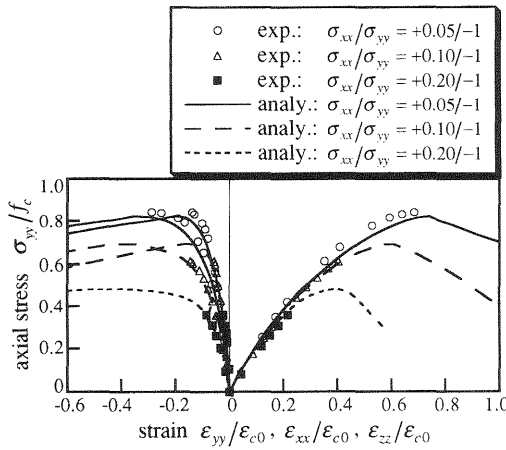


Fig.8. Biaxial compression-tension analyses

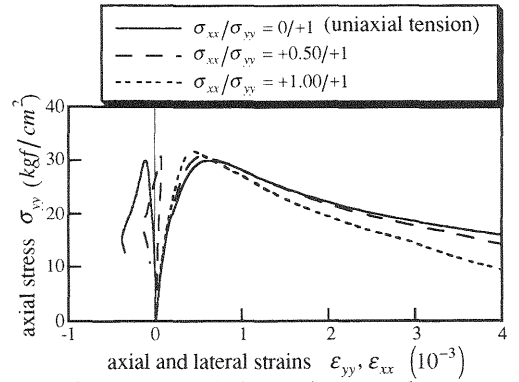
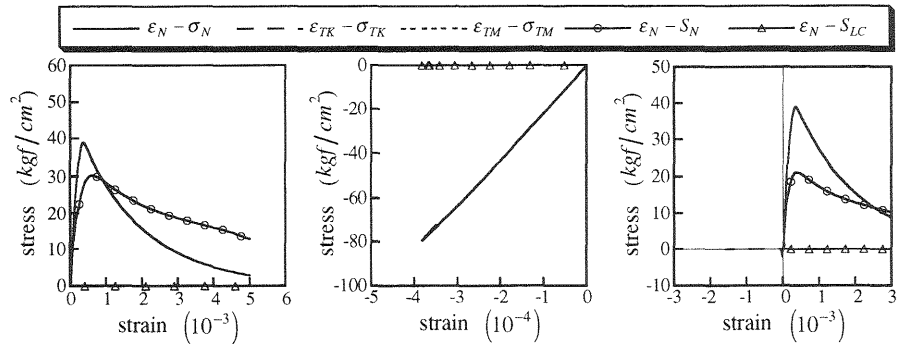


Fig.9. Biaxial tension analyses



(a) microplane 2 (b) microplane 3 (c) microplane 14
Fig.10. Microplane responses for uniaxial tension analysis

in concrete under tension.

The compressive and tensile meridians of failure envelope are evaluated from maximum stresses obtained in the analyses and shown in Fig.11 with experimental results from references (Chen (1982)), where σ_{oct} and τ_{oct} are the octahedral normal and shear stresses. The EMPC Model can predict the compressive meridian very well, however, it slightly overestimates the tensile meridian.

Fig.12 shows the analytical result for the biaxial strength envelope compared with experiments by Kupfer et al. (1969). It confirms that the biaxial strength of concrete can be estimated with accuracy using the present model.

Axial stress σ_{yy} - average volumetric strain ϵ_{qv} relations are shown in Fig.13 for the uniaxial ($\sigma_c/f_c' = 0$) and triaxial ($\sigma_c/f_c' = -0.60$) compression analyses. The volumetric response of the uniaxial compression analysis is consistent with the experimental fact that the volumetric compaction precedes the volumetric dilatation due to axial tensile cracking that corresponds to normal tensile damage on microplane 3 (Fig.5(b)).

- compressive meridian (Balmer)
- compressive meridian (Richart et al.)
- ⊠ tensile meridian (Richart et al.)
- △ equal biaxial compression (Kupfer et al.)
- compressive meridian (Chen)
- - - tensile meridian (Chen)
- ◇ compressive meridian (Smith et al.)
- compressive meridian (analyses)
- ▲ tensile meridian (analyses)

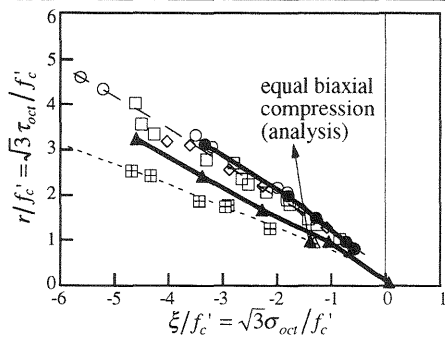


Fig.11. Compressive and tensile meridians

- tests by Kupfer et al.: $f'_c = 190 \text{ kgf/cm}^2$
- tests by Kupfer et al.: $f'_c = 315 \text{ kgf/cm}^2$
- - - tests by Kupfer et al.: $f'_c = 590 \text{ kgf/cm}^2$
- analyses

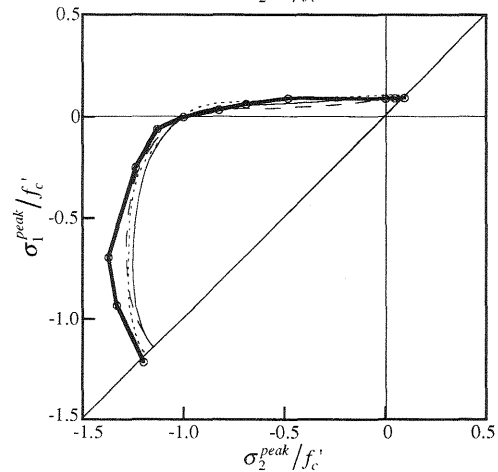
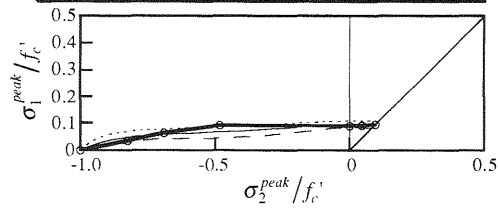


Fig.12. Biaxial strength envelope

It is worth notice that all the present analyses were done with one set of material parameters in spite of the wide range of stress, which verifies the general applicability of the EMPC Model. On the other hand, the optimum fit to experimental results were obtained individually for each stress condition with the previous microplane model in Bazant and Prat (1988), which is not enough to show the versatility (Hasegawa (1994)).

3.2 Cyclic behavior

In Fig.14 the calculated cyclic response under biaxial compression ($\sigma_{xx}/\sigma_{yy} = -0.05/-1$) is compared with the experiment by van Mier (1984). Fig.15 shows the normal, K -shear, and M -shear responses of microplanes 2, 3, and 14 for the analysis. Comparing Fig.14 and 15, it is found that the shape of the macroscopic hysteresis loops, especially the curve in the lower stress level, results from the alternating stress responses between compression and tension on microplanes. This suggests that complicated hysteresis occurs in concrete due to tensile stresses induced in the microscopic levels while no macroscopic tension is applied.

Based on the cyclic biaxial compression analysis as well as cyclic uniaxial and triaxial compression analyses separately performed, the total strain tensor ϵ_{ij} is resolved into elastic ϵ_{eij} and plastic ϵ_{pij} strain tensors considering that the residual strain after complete unloading is the plastic

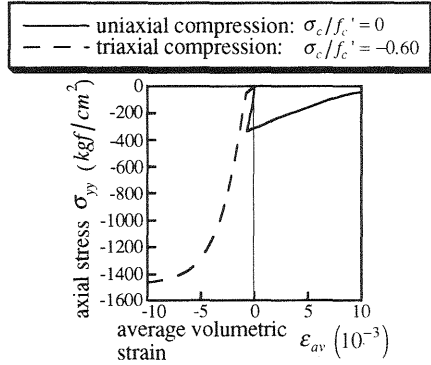


Fig.13. Volumetric behavior

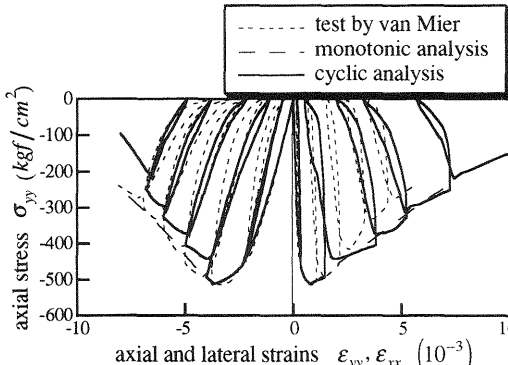
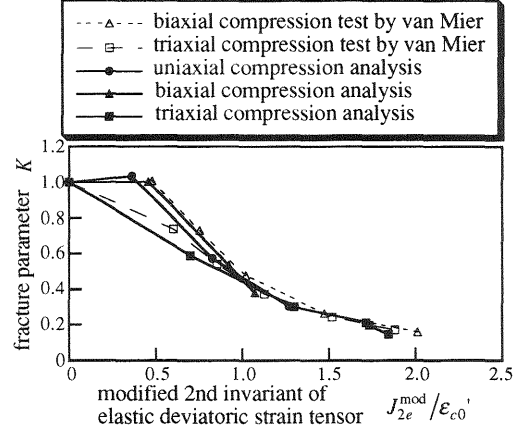
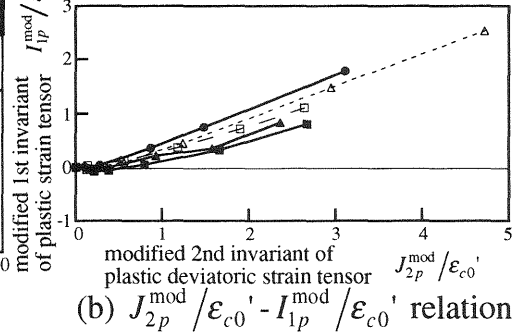


Fig.14. Cyclic biaxial compression analysis

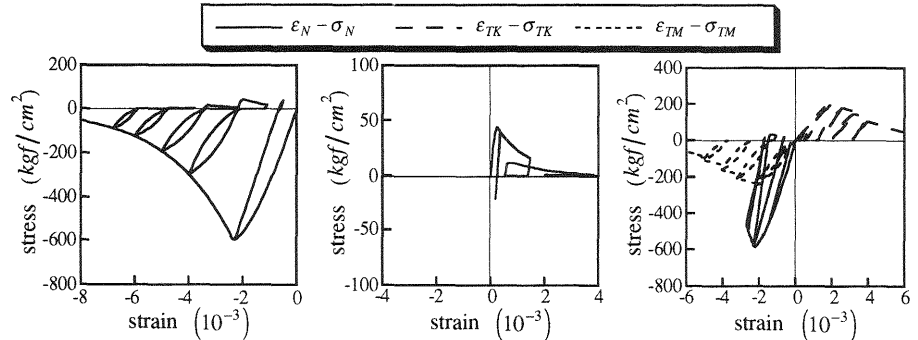


(a) $J_{2e}^{\text{mod}}/\epsilon_{c0}' - K$ relation



(b) $J_{2p}^{\text{mod}}/\epsilon_{c0}' - I_{1p}^{\text{mod}}/\epsilon_{c0}'$ relation

Fig.16. Tensorial invariant relations



(a) microplane 2 (b) microplane 3 (c) microplane 14

Fig.15. Microplane responses for cyclic biaxial compression analysis

strain at the start of unloading. Several invariants were calculated from the tensors. As examples, $J_{2e}^{\text{mod}}/\epsilon_{c0}' - K$ and $J_{2p}^{\text{mod}}/\epsilon_{c0}' - I_{1p}^{\text{mod}}/\epsilon_{c0}'$ relations are shown in Fig.16 comparing with the experimental results by van Mier (1984), where J_{2e}^{mod} and J_{2p}^{mod} : modified 2nd invariants of e_{ij} and e_{pij} ; I_{1p}^{mod} : modified 1st invariant of ϵ_{pij} ; K : fracture parameter; e_{ij} and e_{pij} : elastic and plastic deviatoric strain tensors.

$$J_{2e}^{\text{mod}} = \sqrt{\frac{1}{2} e_{ij} e_{ij}}; J_{2p}^{\text{mod}} = \sqrt{\frac{1}{2} e_{pij} e_{pij}}; I_{1p}^{\text{mod}} = \frac{1}{3} \epsilon_{pii}; K = \frac{J_2^{\text{mod}}}{2G^0 J_{2e}^{\text{mod}}} \quad (18)$$

in which $J_2^{\text{mod}} = \sqrt{s_{ij} s_{ij}/2}$; s_{ij} : deviatoric stress tensor; G^0 : initial shear

modulus. Although the EMPC Model is derived without tensorial invariant relations, it can reproduce the relations as shown in Fig.16, and therefore it can predict cyclic responses with accuracy.

4 Conclusion

The Enhanced Microplane Concrete Model is reconstructed as a more general constitutive law for concrete adapting a few additional static constraints on the microplane. The model can predict not only monotonic but also cyclic responses of concrete with accuracy.

5 Acknowledgment

The author would like to acknowledge the valuable advice of Professors K. Maekawa (The University of Tokyo) and Z. P. Bazant (Northwestern University) during this study.

6 References

- Bazant, Z. P., and Gambarova, P. G. (1984) Crack shear in concrete: Crack band microplane model. *J. Struct. Engrg., ASCE*, 110(9), 2015-2035.
- Bazant, Z. P., and Prat, P. C. (1988) Microplane model for brittle-plastic material: I. Theory, and II. Verification. *J. Engrg. Mech., ASCE*, 114(10), 1672-1702.
- Carol, I., Bazant, Z. P., and Prat, P. C. (1991) Geometric damage tensor based on microplane model. *J. Engrg. Mech., ASCE*, 117(10), 2429-2448.
- Chen, W. F. (1982) *Plasticity in reinforced concrete*. McGraw-Hill Book Company, New York.
- Hasegawa, T. (1994) *Development of the microplane concrete model*. Ph.D. thesis, The University of Tokyo, Tokyo.
- Hasegawa, T., and Bazant, Z. P. (1993) Nonlocal microplane concrete model with rate effect and load cycles. I: General formulation, and II: Application and verification. *J. Mat. in Civ. Engrg., ASCE*, 5(3), 372-410.
- Kupfer, H., Hilsdorf, H. K., and Rusch, H. (1969) Behavior of concrete under biaxial stresses. *J. Amer. Concr. Inst.*, 66(8), 656-666.
- Ozbolt, J., and Bazant, Z. P. (1992) microplane model for cyclic triaxial behavior of concrete. *J. Engrg. Mech., ASCE*, 118(7), 1365-1386.
- Smith, S. S., Willam, K. J., Gerstle, K. H., and Sture, S. (1989) Concrete over the top, or: Is there life after peak? *Amer. Concr. Inst. Mat. J.*, 86(5), 491-497.
- van Mier, J. G. M. (1984) *Strain-softening of concrete under multiaxial loading conditions*. Ph.D. thesis, Eindhoven University of Technology, The Netherlands.